

Cosmic Infrared Background: ISOPHOT FIR source counts at 90, 150 and 180 μm

Mika Juvela¹, Kalevi Mattila¹, and Dietrich Lemke²

¹ Helsinki University Observatory, Helsinki, Finland

² Max-Planck-Institut für Astronomie, Heidelberg, Germany

Abstract. Far-infrared maps obtained with ISOPHOT have been searched for point-like sources. The majority of the 55 sources is believed to be extragalactic and in most cases no previously known sources can be associated with them. Based on the far-infrared spectral energy distributions it is likely that dust-enshrouded, distant galaxies form a significant fraction of the sources.

We estimate the number densities of extragalactic sources at 90 μm , 150 μm and 180 μm wavelengths and at flux density levels down to ~ 100 mJy. The counts are compared with models of galaxy evolution. The counts exceed the predictions of current models, even those with strong evolution, and no-evolution models are rejected at a high confidence level.

Comparison with recent results from COBE mission indicates that at 90 μm the detected sources correspond to $\gtrsim 20\%$ of the extragalactic background light. At longer wavelengths the corresponding fraction is 10%.

1 Introduction

In the far-infrared the cosmic infrared background (CIRB) consists of radiation emitted by galaxies, intergalactic gas and dust, photon-photon interactions (γ -ray vs. CMB) and, possibly, by decaying relic particles. A large fraction of the energy released in the universe since the recombination epoch is contained in the CIRB. An important aspect is the balance between the UV-optical and the infrared backgrounds. With recent observations at infrared and sub-mm wavelengths it has become obvious that star formation efficiencies in the early universe derived from optical and UV observations are underestimated (e.g. Madau et al. [17]; Steidel et al. [24]).

The analysis of the data from the COBE DIRBE (Hauser et al. [6]) and FIRAS (Fixsen et al. [2]) indicated a FIR CIRB flux at a surprisingly high level of ~ 1 MJy sr^{-1} between 100 and 240 μm . Similar results had been obtained already by Puget et al. [19] and Schlegel et al. [22]. Because of the great importance of the FIR CIRB for cosmology these results require confirmation by independent measurements.

The final goal of the ISOPHOT CIRB project is the determination of the FIR CIRB flux level. First steps are the measurement of the CIRB fluctuations and the detection of the bright end of FIR point source population. The

Table 1. The studied fields. The columns are: name of the field, coordinates of the centre of each field, area of the map, name of the ISOPHOT filter used in the observations, number of raster positions observed, step between adjacent raster positions in the staring mode mapping and integration time. The distance of adjacent scans was in all cases identical to the raster step used along the scan line

Field	Map Centre		Area (sq.degr.)	Filter	Rasters	Step (arcsec)	t_{int} (s)
	RA(2000.0)	DEC(2000.0)					
VCN	15 15 21.7	+56 28 58	0.030	C_90	10×4	90	46
				C_135	10×4	90	46
				C_180	10×4	90	46
VCS	15 15 53.1	+56 19 30	0.023	C_90	21×2	90	46
				C_135	21×2	90	46
				C_180	21×2	90	46
NGPN	13 43 53.0	+40 11 35	0.27	C_90	32×4	180	23
				C_135	32×4	180	27
				C_180	32×4	180	27
NGPS	13 42 32.0	+40 29 06	0.53	C_180	15×15	180	32
	13 49 43.7	+39 07 30	0.27	C_90	32×4	180	23
				C_135	32×4	180	27
EBL22	02 26 34.5	-25 53 43	0.19	C_90	32×3	180	23
				C_135	32×3	180	27
				C_180	32×3	180	27
EBL26	01 18 14.5	01 56 40	0.27	C_90	32×4	180	23
				C_135	32×4	180	23
				C_180	32×4	180	23

ISOPHOT CIRB project has potential advantages over the DIRBE analysis: (1) with the much smaller f.o.v. ISOPHOT is capable of looking at the darkest spots between the cirrus clouds; (2) in spite of the smaller f.o.v. ISOPHOT's sensitivity surpasses that of DIRBE in the important FIR window at 120 – 200 μm ; (3) with the good spatial and spectral sampling the galactic cirrus can be separated.

We have mapped four low-cirrus regions at high galactic latitude at the wavelengths of 90, 150, and 180 μm . Here we report on the point sources (galaxies) found in the FIR maps. The FIR source counts are important for the study of the star formation history of the universe and for the testing of models of galaxy evolution.

The point source extraction is based on the fitting of the detector footprint to spatial data. The method is different from those used in most previous studies (e.g. Kawara et al. [10]; Puget et al. [20]) where the source detection has been based on the analysis of the detector signal as a function of time. Our analysis is therefore independent of and complementary to previous results.

2 Observations

The observations were performed with the ISOPHOT (Lemke et al. [13]) aboard ISO (Kessler et al. [11]). The maps were made in the PHT22 staring raster map mode (see Table 1). The area covered is ~ 1.5 square degrees. The fields have low surface brightness and in some cases there is some redundancy i.e. the observed pixel rasters partly overlap each other.

The data were processed with PIA (PHT Interactive Analysis) versions 7.1 and 7.2. The flux density calibration was made using the FCS (Fine Calibration Source) before and after each map. The accuracy of the absolute calibration is expected to be better than 30% (Klaas et al. [12]).

Data reduction from the ERD (Edited Raw Data) to SCP (Signal per Chopper Plateau) was performed using the pairwise method (Stickel [25]). Instead of making linear fits to the ramps consisting of the detector read-outs one examines the distribution of the differences between consecutive read-outs. The mode of the distribution is estimated with myriad technique (Kalluri & Arce [9]) and is used as the final signal for each sky position. The pairwise method is robust against glitches and the analysis was based on the data reduced with this method.

3 Detection procedure

The source detection was performed in two steps using data processed to the AAP (Astrophysical Applications Data) level with PIA and the pairwise method. The data consists of surface brightness values with error estimates. Flat fielding was performed with custom routines.

Each surface brightness value was compared with the mean of the region within a radius of \sim three times the size of the detector pixel. Values more than 0.7σ above the local background were considered as potential point sources. A model consisting of a point source and a constant background was fitted into each region surrounding a candidate position. Footprint matrices were used to calculate the contribution of the point source to the observed surface brightness values. The free parameters of the fit were the source flux density, the two coordinates of the source position, and the background surface brightness. The formal errors are used to calculate the probability, P , that the detection is not caused by background noise.

The completeness of the source detection and the number of false detections were studied with simulations. The results were used to adjust the probability level that was used for discarding uncertain detections. The ratio ρ between the source flux density and the background rms noise, σ_{bg} , was used as a criterion to discard uncertain sources. Since ρ is not directly related to the probability obtained from the footprint fit it can be used as an additional safeguard against false detections.

The actual source list consists of sources detected at two or three wavelengths with a spatial distance between detections of less than $80''$. The expected number of co-incident associations is no more than $\sim 10\%$ and does not significantly affect the source counts.

4 Source counts

The surface density of sources is estimated by dividing the number of detected sources at a given flux density level with the corresponding ‘effective’ map area.

As the first approximation the effective area corresponding to a given flux density level was taken to be the sum of those maps where sources with equal or lower flux densities were detected. The cumulative source densities obtained at $90\mu\text{m}$, $150\mu\text{m}$ and $180\mu\text{m}$ are shown as histograms in Fig. 2. Two sets of sources were used. The first set consists of all detections (dotted line) while in the second set there are only sources detected at more than one wavelength (solid line). The results are similar for $150\mu\text{m}$ and $180\mu\text{m}$ and significant differences are seen only at $90\mu\text{m}$. This is expected, since sources seen at $150\mu\text{m}$ are likely to be seen also at $180\mu\text{m}$ (and vice versa) while more of the $90\mu\text{m}$ sources remain unconfirmed at the longer wavelengths.

A third estimate for the cumulative source densities (dashed lines in Fig. 2) was obtained by selecting sources based on the ratio ρ (see Sect. 3). For each flux density level sources with $\rho > \rho_0$ were selected and no confirmation at other wavelengths was required. The effective area was obtained by integrating the total area where the rms noise was below $1/\rho_0$ times the source flux density. The values of ρ_0 were selected based on simulations. At the bright end the results agree with earlier histograms since no sources are rejected and the corresponding areas converge towards the total area mapped.

At very low flux density levels the small number of sources leads to large uncertainties. The values obtained below 150 mJy for $150\mu\text{m}$ and $180\mu\text{m}$ are probably only indicative.

5 Discussion

5.1 Cirrus confusion

We have checked the probability that some of the sources detected are small scale cirrus structures (cirrus knots). Results of Herbstmeier et al. [7] show that at the scale of the C100 beam size, $d \sim 45''$, the expected cirrus fluctuation amplitude is below $10\text{ Jy sr}^{-1/2}$ for all our $90\mu\text{m}$ maps. According to Gautier et al. [4] this corresponds to a flux density of 4 mJy which is clearly below the flux densities of the faintest $90\mu\text{m}$ detections. Therefore, cirrus is not likely to be a significant contaminant in the source counts although, because of the non-gaussian nature of the cirrus fluctuations (Gautier et al. [4]), our source list may still contain a few cirrus knots.

5.2 Comparison with galaxy spectra

In Fig. 1 we compare the average of the source spectra with the spectra of the galaxies Arp 193 and NGC 4418. In the sample of luminous infrared galaxies presented by Lisenfeld, Isaak & Hills [15] Arp 193 has the lowest and NGC 4418 the highest estimated dust temperature.

In the rest frame the SEDs of luminous infrared galaxies reach maxima between $60\mu\text{m}$ and $100\mu\text{m}$ (Silva et al. [23]; Devriendt, Guiderdoni & Sadat [1]; Lisenfeld, Isaak & Hills [15]). The spectra of our FIR sources are flat in the observed wavelength range and the emission peak is typically above $90\mu\text{m}$. This is consistent with most sources being at redshifts $0.5 \lesssim z \lesssim 1$.

The FIR emission maximum of normal spiral galaxies is also located close to $100\mu\text{m}$ (e.g. Silva et al. [23]). However, in the case of a spiral galaxy a FIR detection at the level of 0.1 Jy would correspond to a visual magnitude brighter than 16 and the optical counterpart should be readily visible. The lack of clear visual counterparts indicates that most of our sources are likely to be more distant and luminous infrared galaxies.

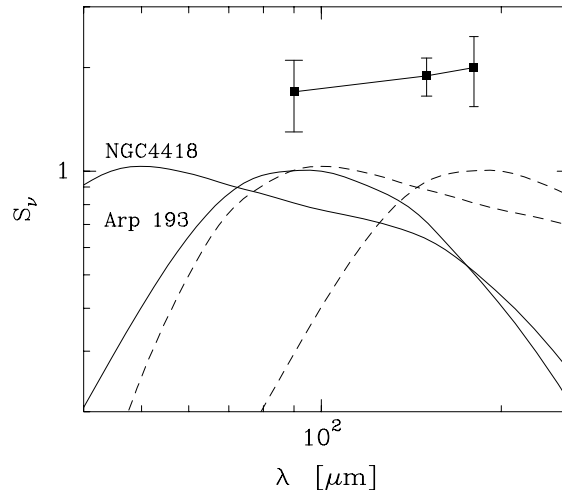


Fig. 1. The average of the source spectra and the model spectra of Lisenfeld et al. ([15]) for the luminous infrared galaxies Arp 193 and NGC 4418. The dashed lines show the spectra of the two galaxies shifted to $z=1.0$. The flux density scale is arbitrary

5.3 Comparison with previous source counts

From Fig. 2 we obtain lower limits of $9 \times 10^4 \text{ sr}^{-1}$, $2.0 \times 10^5 \text{ sr}^{-1}$ and $2.2 \times 10^5 \text{ sr}^{-1}$ for the cumulative source counts $\geq 100 \text{ mJy}$ at $90 \mu\text{m}$, $150 \mu\text{m}$ and $180 \mu\text{m}$,

respectively. Similarly, above 200 mJy the source densities are $1.3 \times 10^4 \text{ sr}^{-1}$, $6 \times 10^4 \text{ sr}^{-1}$ and $7 \times 10^4 \text{ sr}^{-1}$. The dotted histogram, which lies mostly between the two other curves, gives at 100 mJy values $1.4 \times 10^5 \text{ sr}^{-1}$, $2.5 \times 10^5 \text{ sr}^{-1}$ and $3.5 \times 10^5 \text{ sr}^{-1}$ at 90 μm , 150 μm and 180 μm .

Kawara et al. [10] have performed similar counts using ISOPHOT observations of the Lockman Hole. The cumulative source counts were $1.1 \times 10^5 \text{ sr}^{-1}$ and $1.3 \times 10^5 \text{ sr}^{-1}$ at 95 μm and 175 μm , respectively, for sources $S_\nu > 150 \text{ mJy}$. At 90 μm our results are close to their values. Our lowest estimates that were based on detections at two or three wavelengths are, however, lower by more than a factor of two. This could indicate that the requirement of having detections at more than one wavelength does indeed underestimate the counts.

Latest results from the ELAIS survey (Oliver et al. [18]), covering an area of 11.6 square degrees at 90 μm , are similar to the preliminary results reported by Rowan-Robinson et al. [21]. At $\sim 150 \text{ mJy}$ level the source density is $3.3 \times 10^4 \text{ sr}^{-1}$ i.e. a factor of three lower than Kawara et al. [10]. The result is close to our lowest estimate as shown in Fig. 2.

Linden-Vørnle et al. [14] have performed source counts in a 0.4 square degree field at 60 μm and 90 μm . At 90 μm the results are at 100 mJy level similar to the ELAIS counts but are lower at other flux density levels. Also in their re-analysis of the Lockman Hole field they found significantly lower source densities than reported by Kawara et al. [10].

Puget et al [20] have published source counts based on 175 μm ISOPHOT observations of the Marano field covering ~ 0.25 square degrees. The source densities (e.g. $\sim 4 \cdot 10^5 \text{ sr}^{-1}$ at 120 mJy) are slightly higher than our counts.

The source counts obtained in these different ISOPHOT studies are mainly within a factor of ~ 2 from each other but direct comparison is made difficult by the differences in the source flux calibration adopted by the different authors. We have found a $\sim 30\%$ difference between the DIRBE surface brightness values and our data calibrated with PIA version 7.3 (Juvela et al. [8]). This uncertainty is indicated in Fig. 3 by the horizontal lines that are used to represent our source counts. At 90 μm the DIRBE calibration results in lower flux densities and at 150 μm and 180 μm in higher flux densities. These values are better for the comparison with e.g. the results of Oliver et al. [18] at 90 μm since they used DIRBE as the basis of their calibration.

5.4 Comparison with galaxy models

The source counts at 150 μm and 180 μm are much higher than predicted by no-evolution models (e.g. Franceschini et al. [3]). At 180 μm the difference is a factor of five and these models can be safely rejected. Our results indicate that the luminosity or the number of galaxies must evolve strongly with z .

Guiderdoni et al. [5] have presented semi-analytic models for the galaxy evolution. In their model E (which predicts the highest source counts) both the ‘burst’ mode of star formation rate and the relative number of ultraluminous IR galaxies (ULIRGs) increase with z ; at $z = 5$ half of all galaxies are

ULIRGs. The model is in good agreement with extragalactic background light measurements in both optical and infrared. The model predicts source counts of $\sim 1.7 \times 10^5 \text{ sr}^{-1}$ and $\sim 1.8 \times 10^5 \text{ sr}^{-1}$ for sources brighter than 100 mJy at 150 μm and 180 μm , respectively. The number of sources found in this study clearly exceeds these predictions.

Franceschini et al. [3] have presented similar models which include contributions from two galaxy populations: dust-enshrouded formation of early-type galaxies and late-type galaxies with enhanced star-formation at lower redshifts. The predicted source counts at 170 μm are higher than in the model of Guiderdoni et al. [5] and thus in better agreement with our results.

In Fig. 3 we show the predictions of these two models together with counts from other references. For this plot we have selected from Fig. 2 the values of the dotted histogram.

References

1. Devriendt, J.E.G., Guiderdoni, B., Sadat, R. (1999), *A&A*, in press
2. Fixsen, D.J., Dwek, E., Mather, J.C. et al. (1998) *ApJ* **508**, 123
3. Franceschini, A., Andreani, P., Danese, L. (1998) *MNRAS* **296**, 709
4. Gautier, C., III, Boulanger, F., Perault, M., Puget, J.L. (1992) *AJ* **103**, 1313
5. Guiderdoni B., Hivon E., Bouchet F.R., Maffei. B. (1998) *MNRAS* 295, 877
6. Hauser M.G., Arendt R.G., Kelsall T. et al. (1998) *ApJ* **508**, 25
7. Herbstmeier, U., Abraham, P., Lemke, D., et al. (1998) *A&A* **332**, 739
8. Juvela M., Mattila K., Lemke D. (1999) *Cirrus Spectra of Low Surface Brightness Regions*. In: *Proceedings of the Meeting ISO Beyond Point Sources*, ESA-SP
9. Kalluri S., Arce G.R. (1998) *IEEE Transactions on Signal Processing* Vol. **46**, 2, 322
10. Kawara, K., Sato, Y., Matsuhara, H., et al. (1998) *A&A* **336**, L9
11. Kessler M.F., Steinz J.A., Anderegg M.E. et al. (1996) *A&A* **315**, L27
12. Klaas U., Laureijs, R.J., Radovich, M., Schulz, B. (1998) ‘ISOPHOT Calibration Accuracies’, http://www.iso.vilspa.esa.es/manuals/PHT/accuracies/pht_accuracies20/
13. Lemke, D., Klaas, O., Abolins, J., et al. (1996) *A&A* **315**, L64
14. Linden-Vørnle M.J.D., Norgaard-Nielsen H.U., Jorgensen H.E. et al. (1999), submitted to *A&A*
15. Lisenfeld U., Isaak K.G., Hills R. (1999), *MNRAS*, in press, astro-ph/9907035
16. Low, F.J., Cutri R.M. (1994), *Infrared Phys. Technol.* Vol. **35**, No 2/3, 291
17. Madau, P., Ferguson, H.C., Dickinson, M.E., et al. (1996) *MNRAS* **283**, 1388
18. Oliver S., Serjeant S., Efstathiou A., et al., 2000, in ‘ISO Surveys of a Dusty Universe’, Lemke D., Stickel M., Wilke K. (eds.), Springer
19. Puget, J.-L., Abergel, A., Bernard, J.-P. et al. (1996) *A&A* **308**, L5–L8
20. Puget, J.-L., Lagache, G., Clements, D.L., et al. (1999) *A&A* 345, 29
21. Rowan-Robinson, M., Oliver, S., Efstathiou, A., et al. (1999) In: *Proceedings of “The Universe as seen by ISO”*, Paris, ESA SP-427, p. 1011
22. Schlegel D.J., Finkbeiner D.P., Davis M. (1998) *ApJ* **500**, 525
23. Silva L., Granato G.L., Bressan A., Danese L. (1998), *ApJ* **509**, 103
24. Steidel C.C., Adelberger K.L., Giavalisco M. et al. (1999) *ApJ* **519**, 1
25. Stickel, M. (1999) personal communication

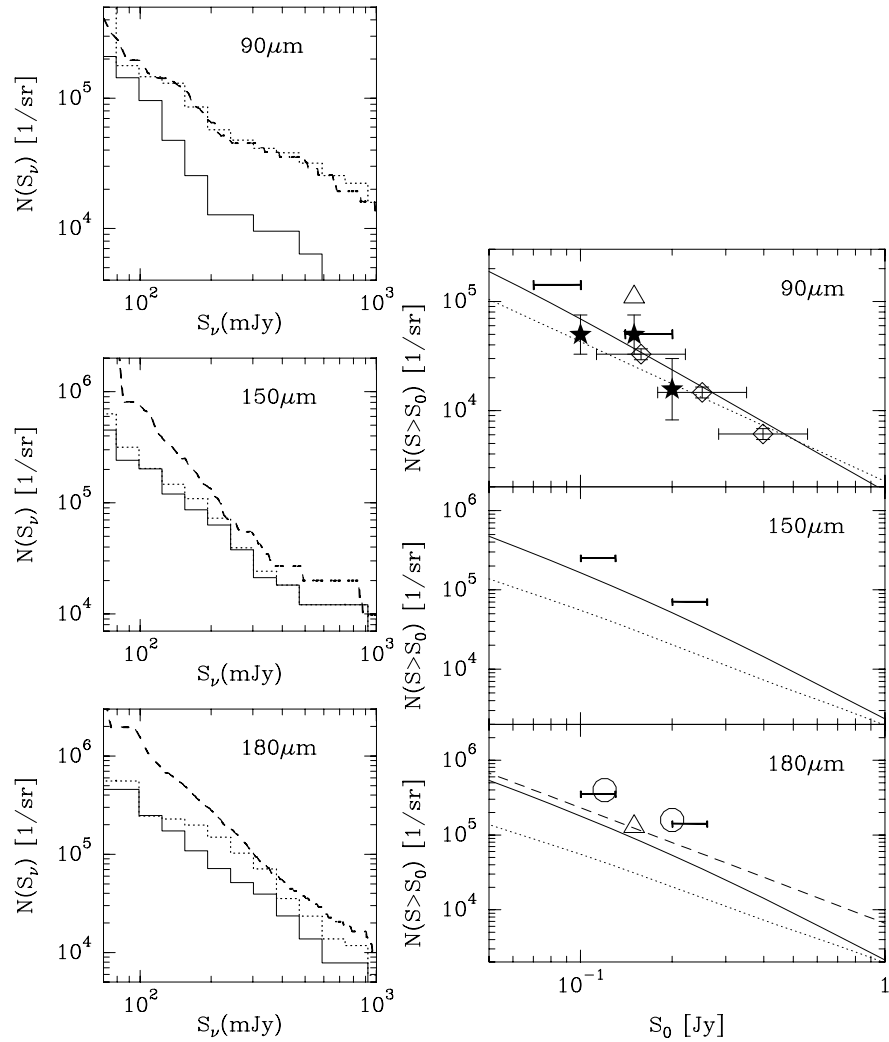


Fig. 2. Cumulative source counts at $90\mu\text{m}$, $150\mu\text{m}$ and $180\mu\text{m}$. The dotted line gives all sources detected and the solid line sources detected at more than one wavelength. Areas were estimated according to the faintest source detected in a map. The dashed curves represent cases in which both the source selection and the area determination were based on the local background fluctuations (see text).

Fig. 3. Comparison with other ISOPHOT counts and models of galaxy evolution. Our source counts at 100mJy and 200mJy are shown together with the results of Puget et al. [20] (circles), Kawara et al. [10] (triangles), Oliver et al. [18] (diamonds) and Linden-Vørnle [14] (stars). We present our results as horizontal lines that indicate the difference between the DIRBE calibration and the adopted ISOPHOT calibration (see text). The predictions of model E of Guiderdoni et al. [5] are shown with solid lines and the evolutionary model of Franceschini et al. [3] with a dashed line. Dotted lines show predictions of no-evolution models ($90\mu\text{m}$: Guiderdoni et al. [5]; $150\mu\text{m}$ and $180\mu\text{m}$: Franceschini et al. [3])